Energy Conversion and Management: X 29 (2026) 101501

Contents lists available at ScienceDirect

Energy Conversion and Management: X

journal homepage: www.sciencedirect.com/journal/energy-conversion-and-management-x

Reliability-driven health-aware control augmentation strategies for wave energy converters

Amin Ziaei *, Hafiz Ahsan Said, John V. Ringwood

Centre for Ocean Energy Research (COER), Department of Electronic Engineering, Maynooth University, Maynooth, Co. Kildare, Ireland

ARTICLE INFO

Keywords:
Control augmentation
Degradation
Health-aware control
Reliability
Wave energy converters

ABSTRACT

Energy-maximising controllers for wave energy converters (WECs) typically exaggerate device motion, which can shorten device longevity and increase operational expenses (OpEx) by reducing maintenance intervals and system reliability. This paper proposes a novel health-aware WEC control structure based on control augmentation to achieve a suitable trade-off between energy maximisation and power take-off (PTO) lifetime enhancement, ultimately leading to a lower levelised cost of energy (LCoE). The main advantage of implementing health-aware WEC control through control augmentation is that the proposed health-aware control paradigm exhibits *versatility* regarding the selection of the nominal (energy-maximising) controller, enabling the selection from a plethora of existing energy-maximising WEC controllers in the literature. Furthermore, two distinct health-aware control augmentation strategies, feedforward and feedback, are proposed, along with analytical derivations of the feasible ranges for their respective augmentation (tuning) parameters. Simulation results demonstrate the versatility of the proposed health-aware control framework when applied with different nominal WEC controllers. Furthermore, a comparative analysis is presented, identifying combinations of augmentation strategies and nominal WEC controllers that yield appealing performance, in terms of lifetime enhancement.

1. Introduction

1.1. Motivation

Renewable energy sources (RESs) are widely regarded as viable alternatives to fossil-fuel-based generation in addressing the increasing impacts of climate change. The global transition towards cleaner energy systems has so far been primarily driven by wind and solar energy, both of which have achieved substantial penetration in modern electricity supply networks. However, the inherent intermittency of these sources means that periods of low wind or solar availability do not always coincide with low electricity demand, which leads to supply–demand mismatch. To avoid such a mismatch, diversification within the RES portfolio is essential to ensure a stable and resilient future clean energy supply system [1].

In this context, wave energy offers a vast and largely untapped RES, with the global potential estimated between 16 000 and 18 500 TWh/year [2], which compares well with global electricity consumption of 27,000 TWh [3]. Beyond its scale, wave energy has been shown to exhibit complementary generation patterns relative to wind and solar resources [4]. This complementarity implies that integrating wave energy into existing renewable-dominated systems could significantly reduce variability in electricity production, thereby enhancing supply security and reducing the need for costly storage or backup generation [5].

Despite its vast resource and potential complementarity benefits, wave energy has yet to achieve commercial success, primarily due to its higher levelised cost of energy (LCoE) compared to more established wind and solar RESs [6]. LCoE is the primary metric for assessing energy-generating technologies, defined as

$$\text{LCoE} = \frac{\text{Capital Expenditure} + \text{Operational Expenditure}}{\text{Produced energy over the plant lifetime}}. \quad (1)$$

The relatively high LCoE for current wave energy technology stems largely from technical challenges. High capital costs arise from full-scale prototyping, testing, and deployment, while high operational costs are driven by the harsh environments in which wave energy converters (WECs), devices used to harness wave energy, operate. Offshore WEC devices, in particular, face additional constraints, as maintenance and repair activities are restricted to limited weather windows [7,8], which can further reduce lifetime energy production. Control technology offers a promising route to minimise LCoE, by

* Corresponding author.
E-mail address: amin.ziaei.2024@mumail.ie (A. Ziaei).

https://doi.org/10.1016/j.ecmx.2025.101501
Received 7 October 2025; Received in revised form 24 December 2025; Accepted 26 December 2025
Available online 29 December 2025

Nomenclature

Abbreviations

HAC	Health-aware control
LiTe – Con	Energy-Maximising Linear Time Invariant Controller
LTI	Linear time-invariant
MPC – SP	Model predictive control with spectral implementation
MPC – ZOH	Model predictive control with zero-order hold implementation
MPC	Model predictive control
MTTF	Mean time to failure
PTO	Power take-off
WEC	Wave energy converter

Symbols

m	Mass of the buoy [kg]
$\boldsymbol{x}_{r(t)}$	State vector of the radiation subsystem
$\boldsymbol{x}(t)$	State vector of the WEC model
$\eta(t)$	Free-surface elevation [m]
γ	Peak shape parameter
$\lambda(t)$	Failure rate (Failures per unit of time)
τ	Learning interval of the health-aware controller
$E_c(t)$	Captured Energy [J]
$f_{ex}(t)$	Wave excitation force [N]
f_{PTO}	Power take-off force [N]
$f_{PTO}^{nom}(t)$	Nominal control input [N]
$f_{PTO}^{ref}(t)$	Reference power take-off force generated by a hydrodynamic controller (control input) [N]
$f_{re}(t)$	Restoring force [N]
$f_r(t)$	Radiation force [N]
H_s	Significant wave height [m]
k	Discrete-time index
m_∞	Added mass at infinite frequency [kg]
N	Prediction steps
n_r	Dimension of radiation state-space model
N_s	Spectral expansion order
q	Trade-off parameter
$R(t)$	Reliability index
s_h	Hydrostatic restoring coefficient [N/m]
t	Time [s]
T_0	Period of the wave excitation force [s]
T_h	Prediction horizon [s]
T_p	Wave peak period [s]
T_s	Sampling interval [s]
$z(t), \dot{z}(t), \ddot{z}(t)$	Heave displacement [m], velocity [m/s] and acceleration [m/s^2]

utilising optimal WEC controllers [9] that aim to maximise energy capture as a surrogate measure for minimising LCoE. However, energy-maximising WEC control actions may drive the WEC into more severe operational states, increasing the range of displacements, velocities, and forces within the system. Such conditions may elevate fault risk and, ultimately, have a detrimental impact on device lifetime.

In general, the risk of failure resulting from component, system, or subsystem faults can be addressed through two distinct control paradigms: *fault-tolerant control* (FTC) and *health-aware control* (HAC) [10]. The FTC paradigm is activated once the system has entered a faulty state and typically relies on a fault detection and identification (FDI) module to provide the diagnostic information necessary for fault accommodation or compensation [11,12]. In contrast, the HAC paradigm is designed for nominal (fault-free) operating conditions and proactively seeks to prevent or delay fault occurrence by continuously monitoring the health status of the system, and incorporating health information into the controller design [13]. Within possible HAC for WECs, power take-off (PTO) system health is the primary focus, as PTO contains most of the moving, energy-converting components, and its degradation is directly influenced by control actions [14]. In contrast, degradation in other subsystems, such as the wave absorber, mooring lines, and sensors, is either independent of control inputs or better addressed using alternative strategies. For example, sensor faults are typically handled via FTC [11,15], while mooring-related issues, such as inertia variation due to biofouling [16], are more suited to adaptive control approaches [17]. Nevertheless, while both FTC and HAC are vital for ensuring the safe and reliable operation of WECs, HAC strategies have received comparatively limited attention in the wave energy control literature [18].

1.2. Related work

For the first time, [18] proposed a general HAC framework for WECs. This framework is motivated by the objective of minimising the LCoE, in (1), under the assumption of constant capital expenditure, i.e. the capital costs are independent of control actions. Given the negative correlation between WEC lifetime and operational expenditure, where an extended lifetime leads to reduced operational costs, a health-aware control law can be formulated as a specific solution to the following multi-objective optimisation problem:

$$\max J = \left[\text{Energy}, \text{Health metric}\right]^\intercal \quad (2)$$
$$\text{s.t.} \begin{cases} \text{Physical constraints}, \\ \text{WEC model}, \end{cases}$$

where the health metric can be represented by widely-used health indicators, such as reliability, remaining useful life (RUL), or accumulated fatigue damage (AFD) [19]. The optimisation problem in (2) yields a Pareto front of non-dominated optimal control laws, necessitating a decision-making algorithm to select the most appropriate control law, based on prevailing conditions. For example, electricity market prices can be used as a criterion to prioritise either extended lifetime or higher energy capture goals.

A key limitation of the structure in (2) is the design complexity: each health-aware control law must be developed from scratch, meaning that existing nominal (energy-maximising) WEC controllers cannot be easily adapted for HAC purposes. To address the complexity issue of the HAC structure in (2), authors in [20] propose a simple health-aware control mechanism that modifies the control input of an existing energy-maximising WEC controller, specifically, a model predictive controller (MPC), to extend PTO lifetime. The control mechanism in [20] is inspired by the control augmentation paradigm, widely used in various applications [21,22], particularly in spacecraft attitude tracking control [23–25], where simple control structures are essential, due to the limited onboard computational resources in spacecraft. In such applications, control augmentation is typically employed to compensate for disturbances, model uncertainties, and nonlinearities; in contrast, [20] uniquely adapts the augmentation concept to the HAC of WECs, with the specific goal of balancing energy capture and PTO lifetime. The proposed control structure in [20] is formulated as Eq. (3) in Box I where the 'Past control information' forms the core of the augmentation mechanism in (3), designed based on the health metric, and q is a trade-off parameter that determines the position along the energy–lifetime trade-off curve shown in Fig. 1. A setting of $q = 0$ in

Health-aware control law = $q \cdot$ Past control information + Nominal control law, (3)

Box I.

(3) corresponds to a purely energy-maximising control strategy. Both HAC architectures are summarised in Fig. 2, where the direct approach corresponds to the health-aware multi-objective control problem in (2), and the indirect approach corresponds to the health-aware control augmentation, which is the focus of this paper. It can be seen that the 'Health metric' is *directly* used in the health-aware control law design in the optimisation-based (direct) approach, while the health metric is *indirectly* used (by modifying 'Past control information') in the control augmentation (indirect) approach.

The primary advantage of the health-aware control augmentation structure is the versatility in the choice of nominal (energy-maximising) controller, which enables the integration of a broad variety of energy-maximising WEC controllers, from simple frequency-domain designs [26] to advanced optimisation-based methods, such as MPC and MPC-like approaches [27]. To this end, complementing [20], this paper investigates this versatility in greater depth, with the aim of evaluating the benefits and drawbacks of incorporating different nominal controllers within the health-aware framework in (3). Furthermore, no analytical results are currently available in [20] to establish the amount of past control information required to render the 'Health-aware control law' in (3) truly health-aware, nor to quantify how this requirement influences the feasible range of the trade-off parameter q.

1.3. Contributions

Therefore, this paper extends the work in [20] with the following key contributions:

- While [20] uses previous values of the 'Health-aware control law' in (3) as the source of past control information (i.e., a feedback control augmentation structure, see Section 4.2), this paper also investigates the potential advantages and drawbacks of using previous values of the 'Nominal control law' as the source of past control information (i.e., a feedforward control augmentation structure, see Section 4.1).
- Derivation of analytical results to determine the required amount of past control information and the feasible range of the trade-off parameter q, in (3), enabling the systematic design of a health-aware control law.
- Demonstration of the versatility of the general control augmentation structure in (3) by implementing and comparing different energy-maximising WEC controllers.

The remainder of the paper is organised as follows: Section 2 recalls the fundamentals of WEC hydrodynamic modelling and develops a state-space representation for a WEC with a degrading PTO. Section 3 presents the subset of nominal WEC controllers utilised here, while Section 4 introduces the proposed HAC augmentation structures based on a PTO reliability (lifetime) metric. Simulation results are presented in Section 5, and concluding remarks are provided in Section 6.

1.4. Notation and preliminaries

$\mathbb{R}$ is the set of real numbers. $\mathbb{Re}(\cdot)$ and $\mathbb{Im}(\cdot)$ denote the real-part and imaginary-part operators. Throughout this paper, j denotes the imaginary unit, i.e., $j^2 = -1$.

$\boldsymbol{I}$ represents the identity matrix:

$$\boldsymbol{I} = \begin{bmatrix} 1 & 0 & \cdots & 0 \\ 0 & 1 & \cdots & 0 \\ \vdots & \vdots & \ddots & \vdots \\ 0 & 0 & \cdots & 1 \end{bmatrix} \in \mathbb{R}^{n\times n}.$$

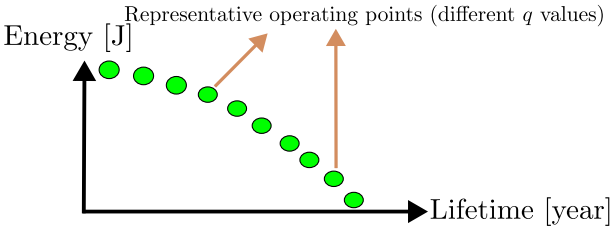

Fig. 1. Schematic illustration of the trade-off between energy capture and lifetime (resulted from the health metric).

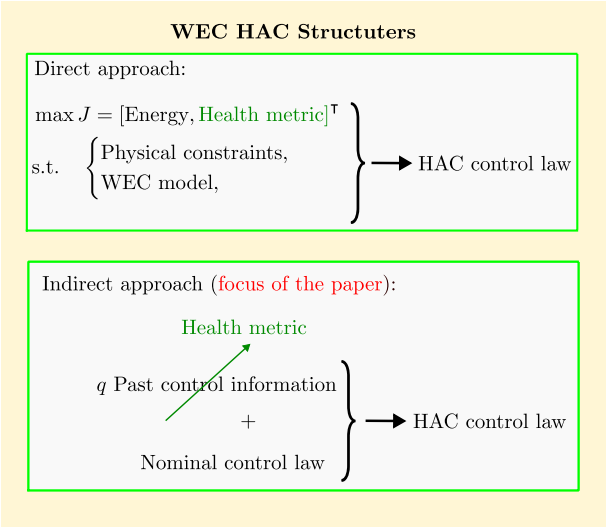

Fig. 2. HAC structures for WECs.

The symbol $\bigoplus$ denotes the direct sum of the n square matrices, that is,

$$\bigoplus_{i=1}^{n} \boldsymbol{A}_i = \begin{bmatrix} \boldsymbol{A}_1 & 0 & \cdots & 0 \\ 0 & \boldsymbol{A}_2 & \cdots & 0 \\ \vdots & \vdots & \ddots & \vdots \\ 0 & 0 & \cdots & \boldsymbol{A}_n \end{bmatrix}. \quad (4)$$

Definition 1. A square matrix $\boldsymbol{A} \in \mathbb{R}^{n\times n}$ is called *Hurwitz* if all of its eigenvalues have strictly negative real parts [28]. That is,

$$\mathbb{Re}(\mu) < 0 \quad \text{for all eigenvalues } \mu \text{ of } \boldsymbol{A}. \quad (5)$$

This condition guarantees that the continuous-time linear system $\dot{\boldsymbol{x}}(t) = \boldsymbol{A}\boldsymbol{x}(t)$ is *asymptotically stable*, meaning that all solutions decay to zero as $t \to \infty$.

2. WEC dynamic modelling

In this section, fundamental concepts of WEC modelling are recalled. First, assuming that the PTO is ideal (healthy), a WEC state-space model is developed in Section 2.1, then PTO degradation is included in the modelling process in Section 2.2. The motion of the

heaving device, depicted in Fig. 3, is written based on Newton's second law:

$$m\ddot{z}(t) = f_{hydro}(z(t), \dot{z}(t), \ddot{z}(t), \eta(t)) - f_{PTO}(t), \tag{6}$$

where m is the mass of buoy and $f_{hydro}(\cdot)$ denotes the total hydrodynamic force acting on the device, expressed as a function of the position $z(t)$, velocity $\dot{z}(t)$, the acceleration $\ddot{z}(t)$ of the body, and free surface wave elevation $\eta(t)$. Furthermore, $f_{PTO}(t)$ is the control force that the PTO unit applies to the body.

It is clear, from (6), that the source of nonlinearity in the model is $f_{hydro}(\cdot)$. Therefore, if assumptions related to linear potential flow theory [29,30] are considered, such as incompressible, inviscid and irrotational flow, $f_{hydro}(\cdot)$ can be written as sum of radiation $f_r(\ddot{z}(t), \dot{z}(t))$, restoring $f_{re}(z(t))$, and wave excitation $f_{ex}(\eta(t))$ forces, as:

$$\begin{cases} f_{hydro}(z(t), \dot{z}(t), \eta(t)) = f_r(\ddot{z}(t), \dot{z}(t)) + f_{re}(z(t)) + f_{ex}(\eta(t)), \\ f_r(\ddot{z}(t), \dot{z}(t)) = -m_\infty \ddot{z}(t) - k_r(t) * \dot{z}(t), \\ f_{re}(z(t)) = -s_h z(t), \\ f_{ex}(\eta(t)) = \eta(t) * k_e(t). \end{cases} \tag{7}$$

In (7), $k_r(t)$ and $k_e(t)$ are the radiation and excitation impulse response functions, respectively. m_∞ is the added mass at infinite frequency, s_h is the hydrostatic restoring coefficient, and $*$ represents the convolution operator. Now, considering (7), (6) is rewritten as:

$$M\ddot{z}(t) = -s_h z(t) - k_r(t) * \dot{z}(t) + f_{ex}(\eta(t)) - f_{PTO}(t), \tag{8}$$

where $M = m + m_\infty$.[1] Note that the hydrodynamic parameters, such as $k_r(t), k_e(t), m_\infty$, and s_h, are typically obtained from boundary element method (BEM) solvers [31] (e.g., NEMOH [32], WAMIT [33]).

Assumption 1. Following conventional practices in simulating ocean wave dynamics (e.g., [34]), the current study models the time-domain excitation force ($f_{ex}(t)$) as a zero-mean periodic signal with period T_0, represented in an N_e-dimensional function space. Therefore, $f_{ex}(t)$ can be written as:

$$f_{\mathrm{ex}}(t) = \sum_{i=1}^{N_e} \alpha_i \cos\left(i\omega_0 t\right) + \beta_i \sin\left(i\omega_0 t\right), \tag{9}$$

where $\omega_0 = \frac{2\pi}{T_0}$ is the fundamental frequency associated with f_{ex}(t).

Assumption 1 provides the periodic characteristic necessary for analytical development of the control augmentation scheme in Section 4. Without Assumption 1, the subsequent analysis, particularly the determination of how much past control information is required to render the augmentation structure in (3) health-aware, would be significantly more difficult.

2.1. WEC modelling with an ideal power take-off

An ideal PTO is defined as follows:

Definition 2 (*Ideal PTO*)**.** A PTO is considered ideal (healthy) if no degradation is present, in which case its output equals the PTO reference signal (control input):

$$f_{PTO}(t) = f_{PTO}^{ref}(t). \tag{10}$$

Using Definition 2 and taking a state vector as $\boldsymbol{x}(t) = \begin{bmatrix} x_1(t) \\ x_2(t) \end{bmatrix} = \begin{bmatrix} z(t) \\ \dot{z}(t) \end{bmatrix}$, the motion equation in (7) is rewritten as:

$$\begin{cases} \dot{x}_1(t) = x_2(t), \\ \dot{x}_2(t) = M^{-1}(-k_r(t) * x_2(t) - s_h x_1(t) + f_{ex}(t) - f_{PTO}^{ref}(t)). \end{cases} \tag{11}$$

[1] From now on, $f_{ex}(t)$ is written instead of $f_{ex}(\eta(t))$ for simplicity.

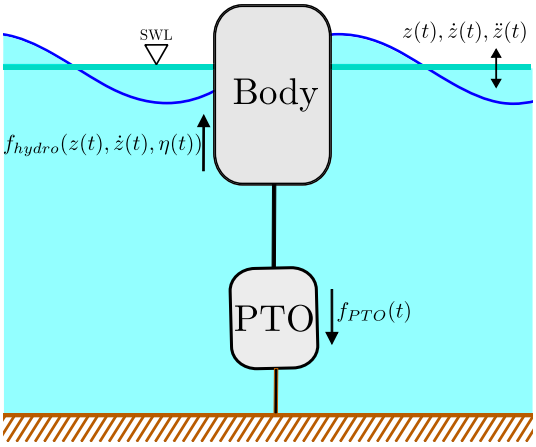

Fig. 3. Simplified illustration of a wave energy converter, operating in a single (heave) degree of freedom. SWL represents still water level.

In the literature on wave energy control [9], it is typical to approximate the convolution term, i.e. $k_r(t) * x_2(t)$, using a linear time-invariant (LTI) system for WEC state-space modelling. Henceforth, the convolution term is approximated, utilising the FOAMM toolbox [35], as:

$$\begin{cases} \dot{\boldsymbol{x}}_{\boldsymbol{r}}(t) = \boldsymbol{A}_{\boldsymbol{r}}\boldsymbol{x}_{\boldsymbol{r}}(t) + \boldsymbol{B}_{\boldsymbol{r}}\dot{z}(t), \\ k_r(t) * x_2(t) \approx \boldsymbol{C}_{\boldsymbol{r}}\boldsymbol{x}_{\boldsymbol{r}}(t), \end{cases} \tag{12}$$

where $\boldsymbol{x}_{\boldsymbol{r}}(t) \in \mathbb{R}^{n_r \times 1}$, with n_r representing the radiation subsystem dimension, is the radiation state vector. In addition, $\boldsymbol{A}_{\boldsymbol{r}}$, $\boldsymbol{B}_{\boldsymbol{r}}$ and $\boldsymbol{C}_{\boldsymbol{r}}$ are the radiation state, input and output matrices with suitable dimensions. Consequently, the complete system state-space model in (11) is rewritten, considering a new state vector $\boldsymbol{x}(t) = [x_1(t), x_2(t), \boldsymbol{x}_{\boldsymbol{r}}(t)]^\intercal \in \mathbb{R}^{(n_r+2)\times 1}$, as:

$$\begin{cases} \dot{\boldsymbol{x}}(t) = \boldsymbol{A}\boldsymbol{x}(t) + \boldsymbol{B}_{\boldsymbol{1}} f_{PTO}^{ref}(t) + \boldsymbol{B}_{\boldsymbol{2}} f_{ex}(t), \\ y_v(t) = \boldsymbol{C}_{\boldsymbol{v}}\boldsymbol{x}(t), \quad y_z(t) = \boldsymbol{C}_{\boldsymbol{z}} x(t), \end{cases} \tag{13}$$

where

$$\begin{cases} \boldsymbol{A} = \begin{bmatrix} 0 & 1 & \boldsymbol{0}_{1\times n_r} \\ -\frac{s_h}{M} & 0 & -\frac{\boldsymbol{C}_{\boldsymbol{r}}}{M} \\ \boldsymbol{0}_{n_r\times 1} & \boldsymbol{B}_{\boldsymbol{r}} & \boldsymbol{A}_{\boldsymbol{r}} \end{bmatrix} \in \mathbb{R}^{(n_r+2)\times(n_r+2)}, \\ \boldsymbol{B}_{\boldsymbol{1}} = -\boldsymbol{B}_{\boldsymbol{2}} = \begin{bmatrix} 0 \\ -\frac{1}{M} \\ \boldsymbol{0}_{n_r\times 1} \end{bmatrix} \in \mathbb{R}^{(n_r+2)\times 1}, \\ \boldsymbol{C}_{\boldsymbol{z}} = \begin{bmatrix} 1 & 0 & \boldsymbol{0}_{1\times n_r} \end{bmatrix}, \boldsymbol{C}_{\boldsymbol{v}} = \begin{bmatrix} 0 & 1 & \boldsymbol{0}_{1\times n_r} \end{bmatrix} \in \mathbb{R}^{1\times(n_r+2)}. \end{cases}$$

Assumption 2. In this study, it is assumed that the system in (13) is observable and controllable. In addition, A is Hurwitz, which guarantees the stability of the system inner dynamics (i.e., $\dot{x}(t) = \boldsymbol{A}x(t)$).

Assumption 2 is consistent with the widely adopted passivity property, valid for all real WEC systems [27].

2.2. WEC modelling with a degrading power take-off

Definition 3 (*Degrading PTO*)**.** When a PTO is degrading, $f_{PTO}^{ref}(t) \neq f_{PTO}(t)$.

Therefore, a mapping between $f_{PTO}^{ref}(t)$ and $f_{PTO}(t)$ needs to be developed, based on a PTO health metric.

In this paper, the health status of the PTO is described using a *reliability index*. Generally, the reliability of a component is described as follows:

Definition 4. Reliability represents the likelihood that a system (or component) will successfully perform its required function over a defined duration, which is defined [36,37] as:

$$R(t) = e^{-\int_0^t \lambda(t)dt}, \quad R \in [0,1] \tag{14}$$

where $\lambda(t)$ represents the failure rate [1/(unit of time)].

The failure rate of a component can be modelled based on its nominal failure rate (λ_0) and the amount of the load ($\ell(t)$) applied to the component [38] as:

$$\lambda(t) = \lambda_0 g(\beta, \ell(t)), \tag{15}$$

where $g(\cdot)$ is the load function, and β is a constant showing the contribution of the applied load to the component failure rate, which is unique for each component. Suppose the considered component is an actuator (i.e., PTO here); in that case, the load parameter will be the control action (i.e., $\ell(t) = f_{PTO}^{ref}(t)$), and the load function can be represented based on the accumulated use of the actuator [39–41] as follows:

$$g(f_{PTO}^{ref}(t)) = 1 + \beta \int_0^t \left| f_{PTO}^{ref}(t) \right| dt. \tag{16}$$

Based on (16), the reliability function in (14) is rewritten as:

$$R(t) = e^{-\int_0^t \lambda_0 \left(1+\beta \int_0^t \left| f_{PTO}^{ref}(t) \right| dt\right) dt}. \tag{17}$$

Now, $f_{PTO}(t)$ can be modelled, based on the reliability metric [42], as:

$$f_{PTO}(t) = R(t) f_{PTO}^{ref}(t). \tag{18}$$

The WEC state-space representation in (13) can now be rewritten as:

$$\begin{cases} \dot{\boldsymbol{x}}(t) = \boldsymbol{A}\boldsymbol{x}(t) + \boldsymbol{B_1} f_{PTO}(t) + \boldsymbol{B_2} f_{ex}(t), \\ y_v(t) = \boldsymbol{C_v}\boldsymbol{x}(t), \quad y_z(t) = \boldsymbol{C_z}\boldsymbol{x}(t), \\ \boldsymbol{B_1} = -\boldsymbol{B_2}, \\ f_{PTO}(t) = R(t) f_{PTO}^{ref}(t), \\ R(t) = e^{-\int_0^t \lambda_0 \left(1+\beta \int_0^t \left| f_{PTO}^{ref}(t) \right| dt\right) dt}. \end{cases} \tag{19}$$

Remark 1. It is worth mentioning that, when $f_{PTO}^{ref}(t) = 0$, nominal reliability is obtained, depending solely on the nominal failure rate λ_0 as:

$$R_0(t) = R(t)\Big|_{f_{PTO}^{ref}(t)=0} = e^{-\lambda_0 t}. \tag{20}$$

3. Nominal WEC controller design

The overall control block diagram of the proposed HAC augmentation structures is shown in Fig. 4. As depicted, a nominal control signal, i.e., $f_{PTO}^{nom}(t)$, is initially generated by a nominal (energy-maximising) WEC controller. Then, the augmentation unit reconfigures $f_{PTO}^{nom}(t)$, by utilising either a feedback or feedforward architecture to generate a PTO reference signal, i.e. $f_{PTO}^{ref}(t)$, with the explicit aim of improving PTO reliability. In this section, the focus is on the $f_{PTO}^{nom}(t)$ design procedure, while the augmentation unit design process is discussed in Section 4.

Remark 2. It should be noted that the nominal controllers in Section 3 only consider the WEC model with an ideal PTO. In other words, the nominal controllers are blind to PTO degradation, and the health-aware reconfiguration mechanism of $f_{PTO}^{nom}(t)$, in Section 4, deals with the WEC model with PTO degradation, as described in Section 2.2.

3.1. Model predictive controllers

In the control literature, MPC is traditionally used for tracking purposes, which means that formulation of the MPC cost function includes the addition of quadratic terms related to tracking error and control effort [43]. Therefore, under specific considerations, tracking MPC formulations typically lead to a convex optimisation problem. However, MPC for WEC application, on the other hand, is primarily developed to maximise captured energy (or minimise negative energy), where the optimisation problem is formulated [27] as:

$$\min_{f_{PTO}^{nom}(t)} J(t) = \int_t^{t+T_h} -x_2(t) f_{PTO}^{nom}(t) dt, \tag{21}$$
$$\text{s.t.} \begin{cases} |x_1(t)| \le x_1^{\max}, \\ \left| f_{\text{PTO}}^{nom}(t) \right| \le f_{PTO}^{\max}, \\ \text{WEC model in (13)}, \end{cases}$$

where T_h is the prediction horizon. Furthermore, x_1^{max} and f_{PTO}^{max} are positive scalars representing the maximum displacement and control force values, respectively.

The optimisation problem, in (21), has two main issues:

1. The optimisation is posed in continuous time, yielding an infinite-dimensional problem that is computationally intractable. Therefore, discretisation of the optimisation problem should be carried out.
2. The optimisation problem in (21) can potentially result in a nonconvex optimisation problem.

Although the first problem is common among all MPC formulations, the second problem is unique to the WEC application, as the primary control objective function is energy maximisation (a bilinear function) rather than tracking error minimisation (a quadratic function).

In the following subsections, it is investigated how the problems associated with (21) can be addressed, either by zero-order hold discretisation and adding an additional term (zero-order hold implementation in Section 3.1.1), or by mapping the optimisation problem to a new parametrisation domain (spectral implementation in Section 3.1.2).

3.1.1. Zero-order hold implementation

Using the zero-order hold discretisation method [44], the WEC state-space model in (13) can be discretised as:

$$\begin{cases} \boldsymbol{x}(k+1) = \boldsymbol{A_d}\boldsymbol{x}(k) + \boldsymbol{B_{1d}} f_{PTO}^{nom}(k) + \boldsymbol{B_{2d}} f_{ex}(k), \\ y_v(k) = \boldsymbol{C_v}\boldsymbol{x}(k), \quad y_z(k) = \boldsymbol{C_z}\boldsymbol{x}(k), \\ \boldsymbol{B_{1d}} = -\boldsymbol{B_{2d}}, \end{cases} \tag{22}$$

where $\boldsymbol{A_d}$, $\boldsymbol{B_{1d}}$, and $\boldsymbol{B_{2d}}$ are discrete versions (zero-order hold equivalent) of $\boldsymbol{A}$, $\boldsymbol{B_1}$, and $\boldsymbol{B_2}$, respectively. Now, the optimisation problem in (21) can be discretised as:

$$\min_{f_{PTO}^{nom}} J = \sum_{k=0}^{N} -x_2(k) f_{PTO}^{nom}(k), \tag{23}$$
$$\text{s.t.} \begin{cases} |x_1(k)| \le x_1^{\max}, \\ \left| f_{\text{PTO}}^{nom}(k) \right| \le f_{PTO}^{\max}, \\ \text{the system in (22)}, \end{cases}$$

where $N = \frac{T_h}{T_s}$ is the number of prediction horizon steps, with T_s the sampling interval. However, the optimisation problem in (23) is still non-convex. A common approach in the literature, to convexify the problem in (23), is to augment the objective function J with additional terms [27]. For example, if the control effort is taken as an extra term [45], the optimisation problem in (23) can be rewritten as:

$$\min_{f_{PTO}^{nom}} J = \sum_{k=0}^{N} -x_2(k) f_{PTO}^{nom}(k) + r f_{PTO}^{nom}(k)^2, \tag{24}$$

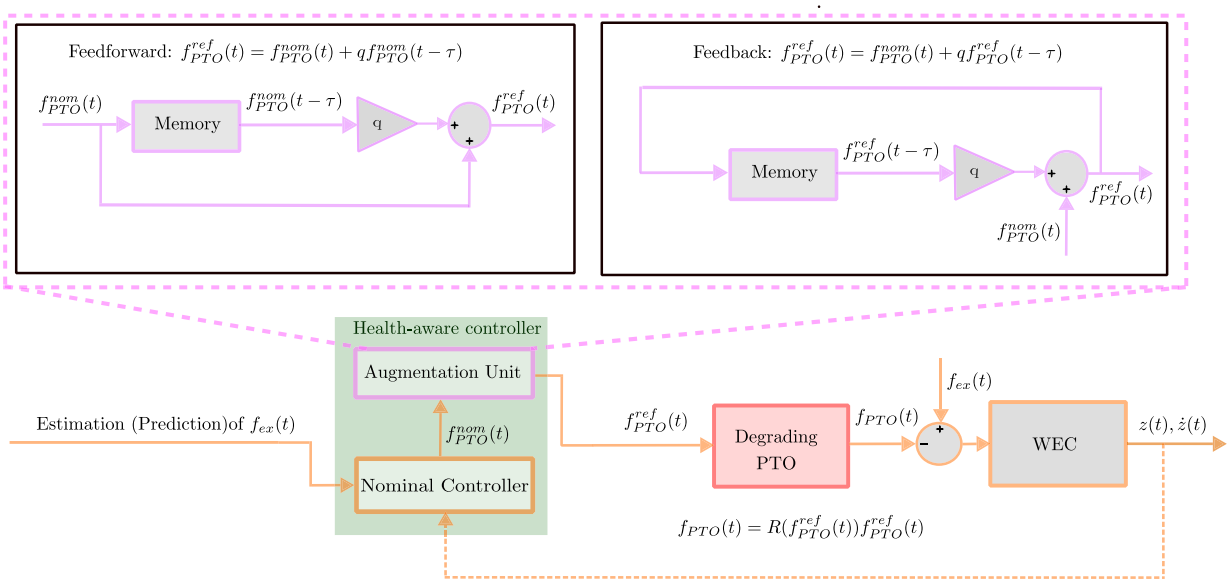

Fig. 4. Block diagram of the proposed health-aware control augmentation using different augmentation structures.

$$\text{s.t.} \begin{cases} \left|x_1(k)\right| \le x_1^{\max}, \\ \left|f_{\text{PTO}}^{nom}(k)\right| \le f_{PTO}^{\max}, \\ \text{the system in (22)}, \end{cases}$$

where r is a positive constant.

Remark 3. It is worth noting that, by defining suitable matrices, such as $\boldsymbol{H}$ and $\boldsymbol{f}$, the performance function J can be represented in the quadratic programming (QP) format (for more information, see, e.g., [45,46]):

$$J = \frac{1}{2}\boldsymbol{F}_{\boldsymbol{PTO}}^{\boldsymbol{nom}\intercal}\boldsymbol{\mathcal{H}}\boldsymbol{F}_{\boldsymbol{PTO}} + \boldsymbol{\mathcal{F}}^{\intercal}\boldsymbol{F}_{\boldsymbol{PTO}}^{\boldsymbol{nom}}, \tag{25}$$

where $\boldsymbol{F}_{\boldsymbol{PTO}}^{\boldsymbol{nom}}$ is the predicted vector of $f_{PTO}^{nom}(k)$. Therefore, under the unconstrained condition, the optimisation problem in (24) admits the following analytical solution, given that $\boldsymbol{\mathcal{H}}$ is symmetric ($\boldsymbol{\mathcal{H}} = \boldsymbol{\mathcal{H}}^T$):

$$\begin{cases} \boldsymbol{F}_{\boldsymbol{PTO}}^{\boldsymbol{nom}} = \boldsymbol{\mathcal{H}}^{-1}\boldsymbol{\mathcal{F}}, \\ f_{PTO}^{nom}(k) = \boldsymbol{F}_{\boldsymbol{PTO}}^{\boldsymbol{nom}}(1), \end{cases} \tag{26}$$

where $\boldsymbol{F}_{\boldsymbol{PTO}}^{\boldsymbol{nom}}(1)$ refers to the so-called receding horizon principle of MPC [47], only the first element of the computed optimal control vector $\boldsymbol{F}_{\text{PTO}}^{\text{nom}}$ is applied to the system, after solving the optimisation problem, in (24), over the prediction horizon.

3.1.2. Spectral implementation

As explained in Section 3.1.1, even though the zero-order hold implementation transforms an infinite-dimensional optimisation problem into a finite-dimensional problem, it does not inherently possess the ability to convexify the optimisation problem without introducing additional regularisation terms. However, spectral implantation not only makes the optimisation problem finite-dimensional, but also convexifies the problem without adding extra terms, which may bias the optimal energy-maximising solution. The main idea behind spectral implementation is to discretise the state vector, control input and wave excitation force by using linear combinations of specific orthogonal basis functions [48,49] as follows:

$$\begin{cases} x_1(t) \approx x_1^{N_s}(t) = \sum_{i=1}^{N_s} \phi_i(t)\hat{x}_{1i} = \boldsymbol{\phi}(t)\hat{\boldsymbol{x}}_1, \\ x_2(t) \approx x_2^{N_s}(t) = \sum_{i=1}^{N_s} \phi_i(t)\hat{x}_{2i} = \boldsymbol{\phi}(t)\hat{\boldsymbol{x}}_2, \\ f_{PTO}^{nom}(t) \approx u^{N_s}(t) = \sum_{i=1}^{N_s} \phi_i(t)u_i = \boldsymbol{\phi}(t)\hat{\boldsymbol{u}}, \\ f_{ex}(t) \approx f_{ex}^{N_s}(t) = \sum_{i=1}^{N_s} \phi_i(t)e_i = \boldsymbol{\phi}(t)\hat{\boldsymbol{e}}, \end{cases} \tag{27}$$

where $\boldsymbol{\phi}(t) = [\phi_1(t), \phi_2(t) \cdots \phi_{N_s}(t)] \in \mathbb{R}^{1\times N_s}$ is a vector of basis functions, with N_s representing the expansion order. In addition, $\hat{\boldsymbol{x}}_{\boldsymbol{1}} = [\hat{x}_{11}, \hat{x}_{12} \cdots \hat{x}_{1N_s}]^{\intercal} \in \mathbb{R}^{N_s\times 1}$, $\hat{\boldsymbol{x}}_{\boldsymbol{2}} = [\hat{x}_{21}, \hat{x}_{22} \cdots \hat{x}_{2N_s}]^{\intercal} \in \mathbb{R}^{N_s\times 1}$, $\hat{\boldsymbol{u}} = [u_1, u_2 \cdots u_{N_s}]^{\intercal} \in \mathbb{R}^{N_s\times 1}$, and $\hat{\boldsymbol{e}} = [e_1, e_2 \cdots e_{N_s}]^{\intercal} \in \mathbb{R}^{N_s\times 1}$ are the spectral-domain vectors of position, velocity, control input, and wave excitation force coefficients, respectively. Considering (11), the WEC spectral domain representation, noting (27), is obtained as:

$$\begin{cases} \dot{x}_1^{N_s}(t) = x_2^{N_s}(t), \\ M\dot{x}_2^{N_s}(t) = -k_r(t) * x_2^{N_s}(t) - s_h x_1^{N_s}(t) + f_{ex}^{N_s}(t) - u^{N_s}(t). \end{cases} \tag{28}$$

The dynamic model in (28) is still infinite-dimensional, due to its dependency on $\boldsymbol{\phi}(t)$. However, defining the following residuals, based on (28), as:

$$\begin{cases} Res_1(t) &= \dot{x}_1^{N_s}(t) - x_2^{N_s}(t), \\ Res_2(t) &= M\dot{x}_2^{N_s}(t) + k_r(t) * x_2^{N_s}(t) \\ &\quad + s_h x_1^{N_s}(t) - f_{ex}^{N_s}(t) + u^{N_s}(t), \end{cases} \tag{29}$$

the dynamic model in (28) becomes finite-dimensional (i.e., of dimension N_s) if the residuals are projected over the orthogonal basis function vector, $\boldsymbol{\phi}(t)$, as follows:

$$\begin{cases} \langle \boldsymbol{\phi}(t)^{\intercal}, Res_1(t)\rangle = \int_0^{T_h} \boldsymbol{\phi}(t)^{\intercal} Res_1(t)dt = 0, \\ \langle \boldsymbol{\phi}(t)^{\intercal}, Res_2(t)\rangle = \int_0^{T_h} \boldsymbol{\phi}(t)^{\intercal} Res_2(t)dt = 0. \end{cases} \tag{30}$$

In this paper, considering Assumption 1, the zero-mean truncated Fourier basis functions are considered as:

$$\boldsymbol{\phi}(t) = \left[\cos\left(\omega_0 t\right), \sin\left(\omega_0 t\right), \ldots, \cos\left(\frac{N_s}{2}\omega_0 t\right), \sin\left(\frac{N_s}{2}\omega_0 t\right)\right], \tag{31}$$

where $N_s = N_e$. After substituting (31) into (28), (30) leads to the following finite-dimensional model [48,50,51]:

$$\boldsymbol{G}\hat{\boldsymbol{x}}_{\boldsymbol{2}} = \hat{\boldsymbol{e}} - \hat{\boldsymbol{u}}, \tag{32}$$

where

$$\begin{cases} \boldsymbol{G} = \bigoplus_{p=0}^{\frac{N_s}{2}} \begin{bmatrix} \mathbb{Re}\{G_0(jp\omega_0)\} & \mathbb{Im}\{G_0(jp\omega_0)\} \\ -\mathbb{Im}\{G_0(jp\omega_0)\} & \mathbb{Re}\{G_0(jp\omega_0)\} \end{bmatrix}, \\ G_0(jp\omega_0) = \boldsymbol{C_v}(jp\omega_0\boldsymbol{I} - \boldsymbol{A})^{-1}\boldsymbol{B_1}, \end{cases} \tag{33}$$

where $G_0(jp\omega_0)$ is the transfer function of (13). Now, the objective function in (23) is represented in the spectral domain as:

$$\begin{aligned} J = \int_0^{T_h} -x_2(t) f_{PTO}^{nom}(t)dt &\approx \int_0^{T_h} -\hat{\boldsymbol{x}}_{\boldsymbol{2}}\boldsymbol{\phi}(t)^{\intercal}\boldsymbol{\phi}(t)\hat{\boldsymbol{u}}dt \\ &= -\frac{T_h}{2}\hat{\boldsymbol{x}}_{\boldsymbol{2}}^{\intercal}\hat{\boldsymbol{u}} \\ &= \frac{T_h}{2}\hat{\boldsymbol{u}}^{\top}\boldsymbol{G}^{-1}\hat{\boldsymbol{u}} - \frac{T_h}{2}\hat{\boldsymbol{u}}^{\top}\boldsymbol{G}^{-1}\hat{\boldsymbol{e}}. \end{aligned} \tag{34}$$

Consequently, the optimisation problem (23) is rewritten in the spectral domain as:

$$\begin{aligned} &\min_{\hat{\boldsymbol{u}}} \frac{T_h}{2}\hat{\boldsymbol{u}}^{\top}\boldsymbol{G}^{-1}\hat{\boldsymbol{u}} - \frac{T_h}{2}\hat{\boldsymbol{u}}^{\top}\boldsymbol{G}^{-1}\hat{\boldsymbol{e}}, \\ &\text{s.t.} \begin{cases} |\boldsymbol{\phi}(t)\hat{\boldsymbol{x}}_{\boldsymbol{1}}| \le x_1^{\max}, \\ |\boldsymbol{\phi}(t)\hat{\boldsymbol{u}}| \le f_{PTO}^{\max}, \\ \boldsymbol{G}\hat{\boldsymbol{x}}_{\boldsymbol{2}} = \hat{\boldsymbol{e}} - \hat{\boldsymbol{u}}. \end{cases} \end{aligned} \tag{35}$$

Remark 4. Similar to the zero-order hold discretisation in Section 3.1.1, there is an analytical spectral solution in the unconstrained condition, noting that $\boldsymbol{G}$ is non-symmetric, obtained from [48] as:

$$\hat{\boldsymbol{u}} = \left(G^{-1} + G^{-\top}\right)^{-1} G^{-1}\hat{e}. \tag{36}$$

However, the optimisation problem becomes infinite-dimensional due to time-dependency of $\boldsymbol{\phi}(t)$ in the constrained condition; therefore, the optimisation problem should be solved at the specific time instants $\{t_p\}_{p=0}^{N_{con}}$, known as colocation points, where N_{con} is the number of time instants.

3.2. LiTe-Con

Unlike the MPC controller in Section 3.1, LiTe-Con is categorised as a non-optimisation-based WEC controller, relying on the well-known impedance matching principle [52]. If the Fourier transform ($\mathcal{F}$) of the motion equation in (11), for the healthy PTO condition (i.e., $f_{PTO}^{ref}(t) = f_{PTO}^{nom}(t)$), is obtained, the force to velocity response yields:

$$\begin{cases} X_2(\omega) = \frac{1}{Z_{imp}(\omega)}\left[F_{ex}(\omega) - F_{PTO}^{nom}(\omega)\right], \\ Z_{imp}(\omega) = \frac{s_h - \omega^2 M + j\omega K_r(\omega)}{j\omega}, \\ K_r(\omega) = B_{rad}(\omega) + j\omega M_a(\omega), \end{cases} \tag{37}$$

where $F_{ex}(\omega)$ is the Fourier transform of $f_{ex}(t)$, $F_{PTO}^{nom}(\omega)$ is the Fourier transform of $f_{PTO}^{nom}(t)$, and $X_2(\omega)$ is the Fourier transform of $x_2(t)$. Also, $Z_{imp}(\omega)$, $B_{rad}(\omega)$ and $M_a(\omega)$ represent the intrinsic impedance of the system, the radiation damping, and added mass, respectively.

LiTe-Con reformulates the impedance-matching principle by deriving the feedforward equivalent, $H_{ff}(\omega)$, of the feedback controller described in [52].

By writing $G_0(\omega) = \mathbb{Re}\{G_0(\omega)\} + j\mathbb{Im}\{G_0(\omega)\}$ where $G_0(\omega) = Z_{imp}^{-1}(\omega)$, $H_{ff}(\omega)$ can be obtained with the following non-parametric representations [52] as:

$$H_{ff}(\omega) = \frac{\mathbb{Re}\{G_0(\omega)\} + j\mathbb{Im}\{G_0(\omega)\}}{2\mathbb{Re}\{G_0(\omega)\}}. \tag{38}$$

Therefore, the feedforward control law is obtained as:

$$F_{PTO}^{nom}(\omega) = H_{ff}(\omega)F_{ex}(\omega). \tag{39}$$

Using frequency-domain identification techniques [53], $H_{ff}(\omega)$ can be approximated by a stable and causal LTI system Σ_1:

$$H_{ff}(\omega) \approx \Sigma_1, \tag{40}$$

where

$$\Sigma_1 : \begin{cases} \dot{\boldsymbol{x}}_{ff}(t) = \boldsymbol{A_{ff}}\boldsymbol{x_{ff}}(t) + \boldsymbol{B_{ff}}f_{ex}(t), \\ f_{PTO}^{nom}(t) = \boldsymbol{C_{ff}}\boldsymbol{x_{ff}}(t). \end{cases} \tag{41}$$

Although the controller dynamics, in (40), are causal and stable, physical constraints are not inherently addressed in this formulation. To incorporate constraint handling, a tunable gain parameter $\kappa \in [0, 1]$ is introduced [52,54], yielding the constrained LiTe-Con formulation as:

$$\Sigma_2 : \begin{cases} \dot{\boldsymbol{x}}_{ff}(t) = \boldsymbol{A_{ff}}\boldsymbol{x_{ff}}(t) + \boldsymbol{B_{ff}}f_{ex}(t), \\ f_{PTO}^{nom}(t) = \kappa\boldsymbol{C_{ff}}\boldsymbol{x_{ff}}(t) + (1-\kappa)f_{\text{ex}}(t). \end{cases} \tag{42}$$

When $\kappa = 1$, the control action follows the unconstrained feedforward dynamics, effectively disabling the constraint-handling mechanism. In contrast, setting $\kappa = 0$ locks the device motion, as the WEC net input force becomes zero, i.e., $f_{ex}(t) - f_{\text{PTO}}^{nom}(t) = f_{ex}(t) - f_{ex}(t) = 0$, leading to zero velocity.[2]

Table 1 summarises all the nominal controllers recalled in the current section, based on their solutions in the constrained and unconstrained scenarios. It can be seen that only LiTe-Con leads to an analytical, although sub-optimal, solution in the constrained case.

4. Health-aware control augmentation

The control augmentation framework is proposed in the following general structure:

$$f_{PTO}^{ref}(t) = q \underbrace{f_h(t)}_{\text{Past control information}} + \underbrace{f_{PTO}^{nom}(t)}_{\text{Nominal control law}}, \tag{43}$$

where $f_h(t)$ is the control history, q is the learning intensity (or trade-off) parameter, and $f_{PTO}^{nom}(t)$ is a nominal (i.e., energy-maximising) control input. Depending on $f_h(t)$, the structure of control augmentation can be feedforward (Section 4.1) or feedback (Section 4.2), as depicted in Fig. 4. Regardless of structure, $f_h(t)$ specifies how much past control information is needed to calculate the overall control law (i.e., $f_{PTO}^{ref}(t)$) health-aware, and *only* q adjusts the intensity of health-awareness. Therefore, the general framework for health-aware control augmentation is governed by the following conditions:

$$\begin{cases} q = 0 & \Rightarrow \text{Energy-maximising WEC control} \\ q \neq 0 & \Rightarrow \text{Health-aware WEC control} \end{cases}$$

In Sections 4.1 and 4.2, the design of $f_h(t)$ and the tuning range of q are fully discussed for feedforward and feedback augmentation structures, respectively.

It is worth mentioning that, regardless of the control augmentation structure, $f_h(t)$ should be designed in a way so that $R(f_{PTO}^{ref}) > R(f_{PTO}^{nom})$ to make f_{PTO}^{ref} in (43) health-aware. Therefore, considering the reliability formula in (17), the global health-aware condition is as follows:

[2] For more information, see [52].

Table 1
Comparison of the solution of the nominal control (NC) strategies under unconstrained and constrained scenarios. ZOH and SP represent zero-order hold and spectral implementations of MPC, respectively.

Condition / NC	Unconstrained	Constrained
MPC-ZOH	$f_{PTO}^{nom}(k) = \boldsymbol{F}_{PTO}^{nom}(1), \quad \boldsymbol{F}_{PTO}^{nom} = \boldsymbol{\mathcal{H}}^{-1}\boldsymbol{\mathcal{F}}$	Numerical solution
MPC-SP	$f_{PTO}^{nom}(t) = \boldsymbol{\phi}(t)\hat{\boldsymbol{u}}, \quad \hat{\boldsymbol{u}} = \left(G^{-1} + G^{-\top}\right)^{-1} G^{-1}\hat{e}$	Numerical solution
LiTe-Con	$f_{PTO}^{nom}(t) = \boldsymbol{C}_{ff}\boldsymbol{x}_{ff}(t)$	$f_{PTO}^{nom}(t) = \kappa \boldsymbol{C}_{ff}\boldsymbol{x}_{ff}(t) + (1-\kappa) f_{\text{ex}}(t)$

Global HAC Condition:

$$R(f_{PTO}^{ref}) > R(f_{PTO}^{nom}) \Longleftrightarrow \int_0^t |f_{PTO}^{ref}|dt < \int_0^t |f_{PTO}^{nom}|dt. \tag{44}$$

Remark 5. The augmentation structure (43) is independent of the particular PTO health metric adopted. In the present paper, PTO health is described by the reliability function $R(\cdot)$, leading to the global HAC condition in (44). The same structure can be combined with alternative health indices, such as accumulated fatigue damage or remaining useful life, which may depend on both the control input and the system states [19]. Whenever the analogue of the global HAC condition in (44) is satisfied for the chosen health metric, the resulting augmented controller is health-aware.

Proposition 1. *If the state vector, under nominal and health-aware cases, is shown with $\boldsymbol{x}_{\boldsymbol{nom}(t)}$ and $\boldsymbol{x}_{\boldsymbol{HAC}(t)}$, respectively, the global HAC condition (44) results in:*

$$\int_0^t |\boldsymbol{x}_{HAC}(t)|dt < \int_0^t |\boldsymbol{x}_{nom}(t)|dt. \tag{45}$$

Proof. Considering Assumption 2, there is a unique $\boldsymbol{P} > 0$ to satisfy the following Lyapunov equation:

$$\boldsymbol{A}^{\intercal}\boldsymbol{P} + \boldsymbol{P}\boldsymbol{A} = -\boldsymbol{Q} \tag{46}$$

where $\boldsymbol{Q} > 0$. Consider a Lyapunov function $V = \boldsymbol{x}^{\intercal}\boldsymbol{P}\boldsymbol{x}$ and the WEC model on (19); then, taking the derivative of the Lyapunov function as:

$$\begin{aligned}
\dot{V} &= \boldsymbol{x}^{\intercal}(\boldsymbol{A}^{\intercal}\boldsymbol{P} + \boldsymbol{P}\boldsymbol{A})\boldsymbol{x} + 2\boldsymbol{x}^{\intercal}\boldsymbol{P}\boldsymbol{B}_{\boldsymbol{1}} f_{PTO} + 2\boldsymbol{x}^{\intercal}\boldsymbol{P}\boldsymbol{B}_{\boldsymbol{2}} f_{ex} \\
&= -\boldsymbol{x}^{\intercal}\boldsymbol{Q}\boldsymbol{x} + 2\boldsymbol{x}^{\intercal}\boldsymbol{P}\boldsymbol{B}_{\boldsymbol{1}} f_{PTO} + 2\boldsymbol{x}^{\intercal}\boldsymbol{P}\boldsymbol{B}_{\boldsymbol{2}} f_{ex}, \\
&\leqslant -\frac{1}{2}\mu_{min}(\boldsymbol{Q})\|\boldsymbol{x}\|^2 + c_1\|\boldsymbol{x}\|^2 + c_2|f_{PTO}|^2 + c_3|f_{ex}|^2, \\
&= -(\frac{1}{2}\mu_{min}(\boldsymbol{Q}) - c_1)\|\boldsymbol{x}\|^2 + c_2|f_{PTO}|^2 + c_3|f_{ex}|^2,
\end{aligned} \tag{47}$$

where $c_1, c_2, c_3 > 0$, and $\mu_{min}(\boldsymbol{Q})$ represents the minimum eigenvalue of $\boldsymbol{Q}$.

Now, with taking integral in $[0, t]$:

$$\begin{aligned}
&V(\boldsymbol{x}(t)) - V(\boldsymbol{x}(0)) \\
&\leqslant -c_0\int_0^t \|\boldsymbol{x}(t)\|^2 dt + c_2\int_0^t |f_{PTO}(t)|^2 dt + c_3\int_0^t \left|f_{\text{ex}}(t)\right|^2 dt,
\end{aligned} \tag{48}$$

where $c_0 = \frac{1}{2}\mu_{min}(\boldsymbol{Q}) - c_1$.

Noting that $V(t) > 0$:

$$\begin{aligned}
&c_0\int_0^t \|\boldsymbol{x}(t)\|^2 dt \\
&\leqslant V(\boldsymbol{x}(0)) + c_2\int_0^t |f_{PTO}(t)|^2 dt + c_3\int_0^t \left|f_{\text{ex}}(t)\right|^2 dt.
\end{aligned} \tag{49}$$

Considering that $V(\boldsymbol{x}(0)) = \|\boldsymbol{x}(0)\|^2$:

$$\begin{aligned}
&\int_0^t \|\boldsymbol{x}(t)\|^2 dt \\
&\leqslant \frac{1}{c_0}\|\boldsymbol{x}(0)\|^2 + \frac{c_2}{c_0}\int_0^t |f_{PTO}(t)|^2 dt + \frac{c_3}{c_0}\int_0^t \left|f_{\text{ex}}(t)\right|^2 dt.
\end{aligned} \tag{50}$$

Finally, considering the HAC condition in (44), and defining health-aware $f_{PTO} = R(f_{PTO}^{ref})f_{PTO}^{ref} \rightarrow \boldsymbol{x}_{HAC}$ and nominal $f_{PTO} = R(f_{PTO}^{nom})f_{PTO}^{nom} \rightarrow \boldsymbol{x}_{nom}$ cases, one can get:

$$\int_0^t |\boldsymbol{x}_{HAC}(t)|dt < \int_0^t |\boldsymbol{x}_{nom}(t)|dt, \tag{51}$$

which completes the proof. □

From a physical standpoint, WEC degradation is closely associated with exaggerating device motion. Proposition 1 therefore shows that the objective of the health-aware controller is to compensate for degradation by actively mitigating motion exaggeration.

4.1. Feedforward control augmentation strategy

For the feedforward structure, considering $f_h(t) = f_{PTO}^{nom}(t-\tau)$, (43) is rewritten as:

$$f_{PTO}^{ref}(t) = f_{PTO}^{nom}(t) + q f_{PTO}^{nom}(t-\tau), \tag{52}$$

where $\tau \in [0, \infty)$ is the learning interval from the previous nominal control information.

Lemma 1. *Considering Assumption 1 and the linear model without PTO degradation in (13), the nominal PTO force, $f_{PTO}^{nom}(t)$, as the output of a linear nominal WEC controller, remains periodic with the same period as the excitation force, $f_{ex}(t)$ (i.e., T_0).*

Proof. Please see Appendix. □

Theorem 1. *Considering Lemma 1 and the global HAC condition in (44), $f_{PTO}^{ref}(t)$, calculated from (52), is health-aware with $\tau = T_0$ if $q \in [-1, 0)$.*

Proof. Using the periodicity characteristic in Lemma 1, (52) yields:

$$\begin{aligned}
f_{PTO}^{ref}(t) &= f_{PTO}^{nom}(t) + q f_{PTO}^{nom}(t-T_0) \\
&= f_{PTO}^{nom}(t) + q f_{PTO}^{nom}(t) \\
&= (1+q) f_{PTO}^{nom}(t).
\end{aligned} \tag{53}$$

Therefore, considering the global HAC condition in (44), $\int_0^t |f_{PTO}^{ref}|dt < \int_0^t |f_{PTO}^{nom}|dt$ if $q \in [-1, 0)$, which completes the proof. □

Corollary 1. *Maximum reliability, under the feedforward control augmentation structure in (52), is obtained when $q = -1$ as:*

$$R_{max}^{ff}(t)\Big|_{\text{Feedforward (52)}} = R_0(t). \tag{54}$$

Proof. Considering (53), f_{PTO}^{ref} becomes zero when $q = -1$. So, the maximum reliability (i.e., R_{max}) equals nominal reliability in (20) (i.e., R_0), which completes the proof. □

4.2. Feedback control augmentation strategy

For the feedback structure, consider $f_h(t) = f_{PTO}^{ref}(t-\tau)$, (43) can be rewritten as:

$$f_{PTO}^{ref}(t) = f_{PTO}^{nom}(t) + q f_{PTO}^{ref}(t-\tau). \tag{55}$$

Theorem 2. *Considering Lemma 1 and the global HAC condition in (44), $f^{ref}_{PTO}(t)$, calculated from (55), is health-aware with $\tau = T_0$ if $q \in (-1, 0)$.*

Proof. Using recursive expansion, (55) yields:

$$\begin{aligned} f^{ref}_{PTO}(t) &= q\, f^{ref}_{PTO}(t-\tau) + f^{nom}_{PTO}(t) \\ &= q^2 f^{ref}_{PTO}(t-2\tau) + q\, f^{nom}_{PTO}(t-\tau) + f^{nom}_{PTO}(t) \\ &= \cdots \\ &= q^n f^{ref}_{PTO}(t-n\tau) + \sum_{i=0}^{n-1} q^i f^{nom}_{PTO}(t-i\tau). \end{aligned} \tag{56}$$

Therefore, taking the limit as $n \to \infty$ (that is, steady-state), $f^{ref}_{PTO}(t)$ becomes unbounded unless $|q| < 1$. So, with $|q| < 1$, the steady-state control input can written as:

$$f^{ref}_{PTO}(t) = \sum_{i=0}^{\infty} q^i f^{nom}_{PTO}(t-i\tau). \tag{57}$$

Now, Lemma 1 leads to:

$$\begin{aligned} f^{ref}_{PTO}(t) &= \sum_{i=0}^{\infty} q^i f^{nom}_{PTO}(t-iT_0) \\ &= \sum_{i=0}^{\infty} q^i f^{nom}_{PTO}(t) < \frac{1}{1-q} f^{nom}_{PTO}(t). \end{aligned} \tag{58}$$

Therefore, considering the global HAC condition in (44), $\int_0^t |f^{ref}_{PTO}|dt < \int_0^t |f^{nom}_{PTO}|dt$ if $q \in (-1, 0)$, completing the proof. □

Corollary 2. *Maximum reliability, under the feedback control augmentation structure in (55), is obtained when $q \to -1$ as:*

$$\begin{cases} R^{fb}_{max}(t)\Big|_{Feedback\ (55)} = \lim_{q\to -1} R(t) = \theta(t) R_0(t) < R_0(t), \\ \theta(t) = e^{-\frac{1}{2}\beta\lambda_0 \int_0^t \left(\int_0^t \left|f^{nom}_{PTO}(t)\right| dt\right) dt}. \end{cases} \tag{59}$$

Proof. Considering (58), $|f^{ref}_{PTO}(t)| < \lim_{q\to -1} \frac{1}{1-q} |f^{nom}_{PTO}(t)| \approx \frac{1}{2}|f^{nom}_{PTO}(t)|$. Therefore, substituting $|f^{ref}_{PTO}(t)| \approx \frac{1}{2}|f^{nom}_{PTO}(t)|$ into the reliability formula in (17), one can get:

$$\begin{aligned} \lim_{q\to -1} R(t) &= \lim_{q\to -1} e^{-\int_0^t \lambda_0 \left(1+\beta \int_0^t \left|f^{ref}_{PTO}(t)\right| dt\right) dt}, \\ &\approx e^{-\int_0^t \lambda_0 \left(1+\frac{1}{2}\beta \int_0^t \left(\int_0^t \left|f^{nom}_{PTO}(t)\right| dt\right) dt\right) dt}, \\ &= e^{-\lambda_0 t} e^{-\frac{1}{2}\beta\lambda_0 \int_0^t \left(\int_0^t \left|f^{nom}_{PTO}(t)\right| dt\right) dt}, \\ &= R_0(t) e^{-\frac{1}{2}\beta\lambda_0 \int_0^t \left(\int_0^t \left|f^{nom}_{PTO}(t)\right| dt\right) dt} < R_0(t), \end{aligned} \tag{60}$$

completing the proof. □

Remark 6. It is worth noting that the feedforward structure offers greater flexibility in achieving maximum reliability, since $R^{fb}_{max}(t) < R^{ff}_{max}(t) = R_0(t)$.

Remark 7. It is worth noting that adaptive WEC controllers [17,55], which update model parameters or device characteristics online, can also be considered as a nominal controller. The proposed health-aware augmentation structure can accommodate any nominal control law, so adaptive WEC control approaches, in addition to the proposed fixed-model energy-maximising WEC controllers, are compatible with the proposed health-aware control structure.

5. Simulation results

5.1. Model setup and simulation parameters

This study employs a heaving point absorber WEC, illustrated in Fig. 5, together with its main dimensions. Both irregular and regular wave conditions are considered. The irregular waves are stochastically generated from a JONSWAP spectrum [57], characterised by a significant wave height of $H_s = 2.5$ m, a peak period of $T_p = 10.5$ s, and a peak enhancement factor of $\gamma = 3.3$. These parameters approximate the most frequently occurring sea state at the Atlantic Marine Energy Test Site (AMETS), Berth A, located off the north-west coast of Ireland [58] (see Fig. 6).

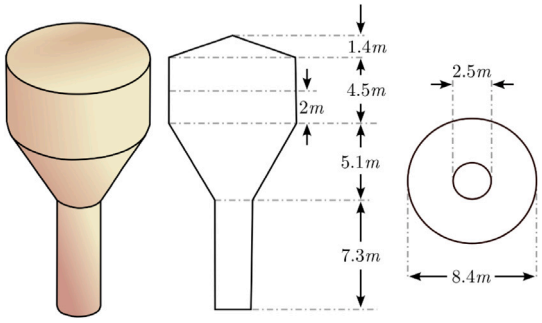

Fig. 5. Schematic illustration of the point absorber WEC device in the current study [56].

Table 2
Simulation parameters.

WEC	
Total mass M	1.4706×10^5 [kg]
Hydrostatic stiffness s_h	5.57×10^5 [N/m]
Radiation subsystem dimension n_r	6
Physical constraints	
Maximum position x_1^{max}	2 [m]
Maximum control input f^{max}_{PTO}	1×10^6 [N]
Nominal control parameters	
Sampling interval T_s	0.1 [s]
Prediction horizon N (MPC-ZOH)	100 steps
Regularisation parameter r (MPC-ZOH)	4×10^{-8}
Basis function expansion order N_s (MPC-SP)	66
Optimisation algorithm (MPC-ZOH & MPC-SP)	MATLAB-quadprog
Constraint-handling gain κ (LiTe-Con)	0.05
Health-aware control parameters	
Learning interval τ	10.5 [s]
Learning intensity (or trade-off parameter) q	$\{0, -0.1, -0.5, -0.9, -1\}$
PTO reliability parameters	
λ_0 (Direct drive PTO [61])	0.93 [failures/year]
β	10^{-13}

In addition, regular waves are considered to reveal better the essence of the health-aware calculations in Section 4. Following [59], regular waves can be modelled as:

$$\begin{cases} f_{ex}(t) = A^* \cdot \sin\left(\frac{2\pi}{T_p} t\right), \\ A^* = \left|K_e\left(\frac{2\pi}{T_p}\right)\right| \frac{H_s}{2}, \end{cases} \tag{61}$$

where K_e is the Fourier transform of the excitation impulse response function, k_e in (7). The full set of simulation parameters is provided in Table 2.

Finally, in this paper, to focus on the main contribution, namely the development of health-aware control augmentation strategies, full present and future knowledge of $f_{ex}(t)$ is assumed for the design of the nominal controllers, in order to simplify the analysis. In a practical scheme, an unknown-input estimator would be used to estimate $f_{ex}(t)$ [50], with an autoregressive model [60] used to forecast future values.

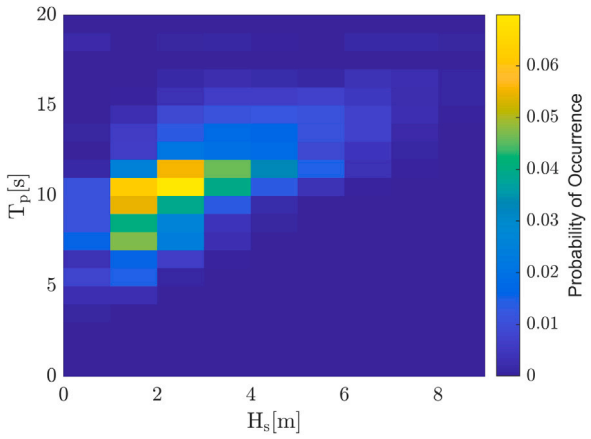

Fig. 6. Significant wave height H_s and significant period T_p occurrences at the Atlantic Marine Energy Test Site (AMETS) Berth A site, based on 30 min (H_s, T_p) wave buoy data collected by Marine Institute [58].

5.2. Health-aware control performance

This section investigates the performance of the proposed health-aware control augmentation strategy, in terms of the trade-off between energy capture and PTO lifetime. Simulation results are calculated over a one-week period, with results then extrapolated over a six-year period, considering both regular and irregular wave conditions. By comparing different nominal controllers, embedded within the augmentation structure, the analysis provides insights into how the choice of q, the augmentation structure, and the nominal controller affect overall health-aware control performance.

To quantitatively assess PTO lifetime, the well-known mean time to failure (MTTF) metric [36] is employed throughout this section. MTTF is defined as the integral of the reliability function $R(t)$ over time, i.e.,

$$\text{MTTF} = \int_0^\infty R(t)\,dt. \tag{62}$$

5.2.1. Results for regular wave excitation

Fig. 7 illustrates the relationship between captured energy and MTTF for different values of the trade-off parameter q, for the regular wave condition, when various nominal controllers are embedded within the proposed feedback augmentation structure detailed in Section 4. Each data point represents the outcome of a six-year extrapolation of the one-week simulation data for both reliability and energy, where the reliability decay of the PTO subsystem is evaluated alongside the total extracted energy. The inset plots highlight the evolution of reliability and energy for a representative case (i.e., the green box in Fig. 7), showing how the MTTF is derived from the reliability function $R(t)$, while energy is accumulated over the same operational period.

The results confirm that the trade-off parameter q plays a crucial role in shaping health-aware control performance. For smaller values of q, the health-aware controller prioritises energy maximisation, as expected, resulting in higher energy yield but accelerated degradation and shorter MTTF. As q increases, the augmented control law (f_{PTO}^{ref}) places a greater emphasis on preserving PTO health, which extends MTTF, albeit at the cost of reduced energy capture. The trade-off across all controllers reflects the flexibility of the proposed framework in adjusting operational priorities between aggressive energy production and conservative, reliability-driven operation.

In terms of controller-specific behaviour, the MPC-SP nominal controller delivers the highest energy yield for aggressive operation (low MTTF) among the three controllers considered. Compared to the other controllers, MPC-SP exhibits the largest shift along the energy–lifetime curve, indicating that its performance can be more effectively tuned through the trade-off parameter, q. LiTe-Con, in contrast, consistently favours longer lifetimes with lower energy capture, due to its inherently more conservative nature. MPC-ZOH provides an intermediate balance between energy and MTTF; however, due to convexity limitations in the optimisation problem, MPC-ZOH cannot be employed for certain trade-off values, such as $q = -0.9$.

Fig. 8 shows the corresponding energy–MTTF trade-offs for the feedforward augmentation structure. As with the feedback case, each point represents a six-year extrapolation of the one-week simulation data, evaluating both energy capture and reliability simultaneously. The same general trend is observed: decreasing q favours energy maximisation at the expense of shorter lifetime, while increasing q extends MTTF at the cost of reduced energy. There are, however, some notable differences compared to the feedback structure. Firstly, for the feedforward case, extreme trade-off values of $q = -1$ can be employed for both MPC-SP and LiTe-Con (see Remark 6), whereas MPC-ZOH continues to suffer from convexity issues and cannot be stably applied for $q = -1$. Secondly, all nominal controllers achieve greater lifetime extension under feedforward augmentation than in the feedback case, as shown in Fig. 7, highlighting the ability of the feedforward structure to provide more flexibility in terms of the trade-off between captured energy and PTO reliability.

5.2.2. Results for irregular wave excitation

Figs. 9 and 10 present the energy–MTTF trade-offs for the irregular wave condition, for the feedback and feedforward control augmentation structures, respectively. Compared to the regular case (Figs. 7–8), convexity issues become more pronounced for MPC-ZOH, where MPC-ZOH cannot be calculated for $q < -0.1$ within the tested simulation range for q, i.e., $q \in \{0, -0.1, -0.5, -0.9, -1\}$. On the other hand, health-aware results for LiTe-Con and MPC-SP cannot be achieved for $q = -0.9$ for the feedback structure, and $q = -0.9$ and $q = -1$ for the feedforward structure. Therefore, Figs. 9 and 10 highlight the challenges of extending the augmentation scheme to irregular wave environments for larger q values.

The root cause of less freedom for q selection in the irregular wave case can be explained by examining the role of the delay parameter τ in the augmentation structure. For the regular wave case, the delay $\tau = T_p = 10.5$ [s] is perfectly aligned with the period of the excitation force, resulting in a global destructive effect on the control input (i.e., $\forall t \in \mathbb{R} \quad |f_{PTO}^{ref}(t)| < |f_{PTO}^{nom}(t)|$) that enhances PTO health, when high q values are selected. However, for the irregular wave case, the excitation force $f_{ex}(t)$ contains multiple frequency components, and the fixed delay τ, chosen based on the peak period of the wave spectrum, cannot align with the multiple frequency components present in irregular waves. As a result, the intended destructive interference of the control augmentation scheme cannot be perfectly achieved. For further clarification, Fig. 11 shows control input evolution for different q values, using the feedforward structure with MPC-SP as the nominal controller. It is clear that, for the regular wave case, increasing q reduces the resulting control input $f_{PTO}^{ref}(t)$, ensuring the global HAC condition in (44). However, in the irregular wave case, increasing q results in constructive behaviour in the control input calculation (i.e., the green box in Fig. 11). Also, the constructive effect is relatively small for smaller q values, and satisfies the global HAC condition in (44), more negative q values, such $q = -0.9$ and $q = -1$, result in severe constraint violation; therefore, a health-aware control law cannot be computed to satisfy the condition in (44). Consequently, in irregular waves, the current augmentation scheme requires further investigation to ensure health-aware operation for large negative q values. One possible approach could be to develop an event-triggered mechanism [25] that selectively deactivates the learning from past control information ($\tau = 0$) when $|f_{PTO}^{ref}| > |f_{PTO}^{nom}|$. While such an event-triggered mechanism could extend the operational freedom of health-aware control in irregular waves, its development lies beyond the scope of this paper, which primarily focuses on introducing the health-aware control augmentation strategy and highlighting its advantages and limitations with different nominal WEC controllers and augmentation structures (i.e., feedback and feedforward).

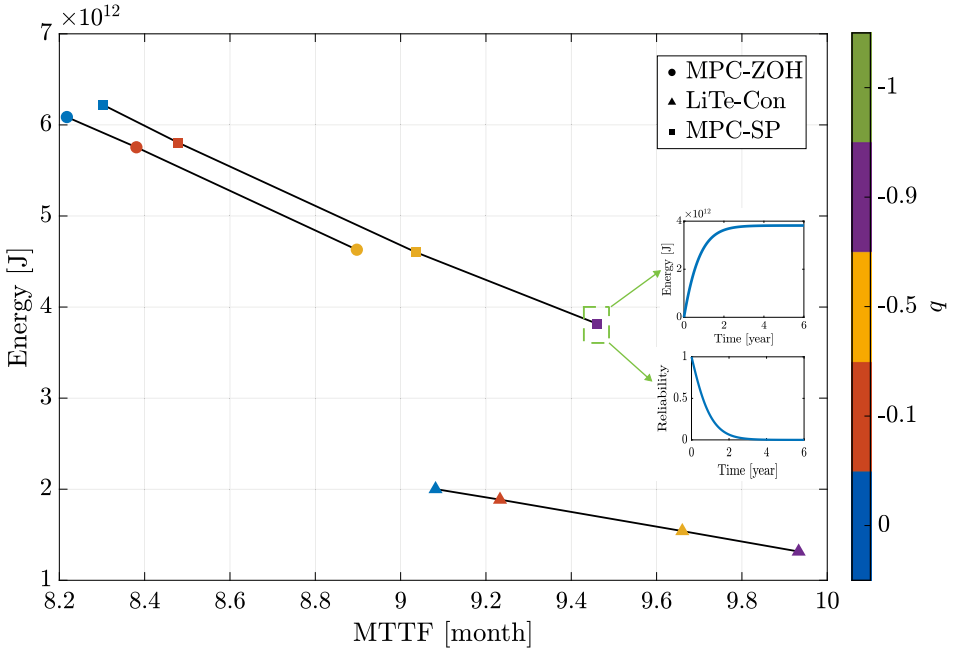

Fig. 7. Energy and MTTF values for a six-year period and different q in the regular wave condition. Various controllers, such as the MPC-ZOH (circle), MPC-SP (square), and LiTE-Con (triangle), are utilised as nominal controllers within the feedback control augmentation structure.

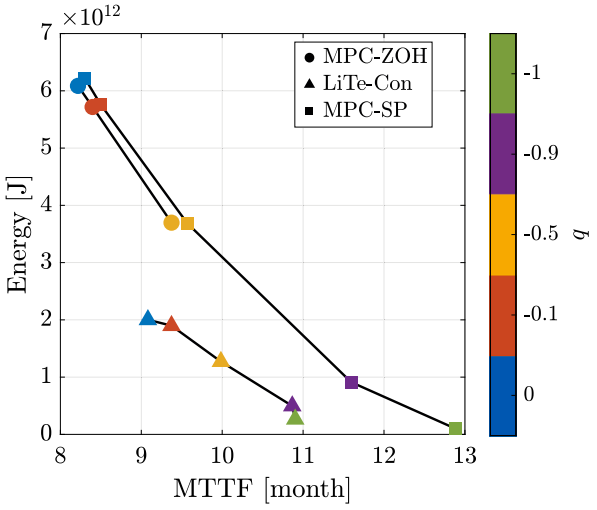

Fig. 8. Energy and MTTF values for a six-year period and different q in the regular wave condition. Various controllers, such as the MPC-ZOH (circle), MPC-SP (square), and LiTE-Con (triangle), are utilised as nominal controllers within the feedforward control augmentation structure.

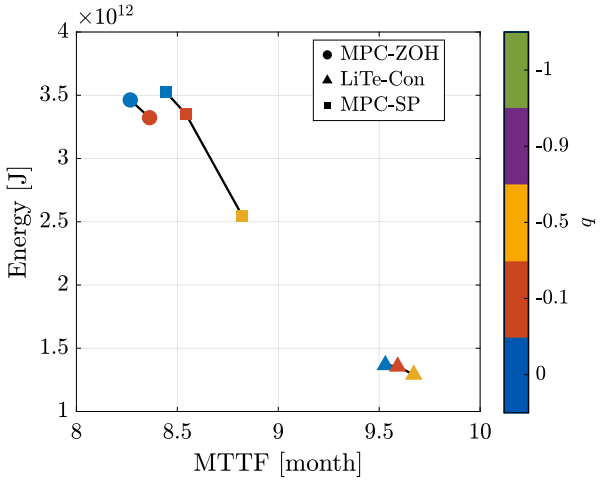

Fig. 9. Energy and MTTF values for a six-year period and different q in the irregular wave condition. Various controllers, such as the MPC-ZOH (circle), MPC-SP (square), and LiTE-Con (triangle), are utilised as nominal controllers within the feedback control augmentation structure.

6. Conclusion

This paper presents a health-aware control augmentation framework for WECs, designed to balance captured energy against the PTO lifetime. By embedding various energy-maximising WEC controllers within both feedback and feedforward augmentation structures, the proposed approach provides a versatile means to make existing energy-maximising WEC controllers health-aware, by modulating WEC operation between aggressive energy capture and reliability-driven safe operation. Simulation results for regular and irregular wave conditions confirm the effectiveness of the framework in shaping the trade-off between energy and lifetime through the selection of the augmentation parameter q. For both (regular and irregular) wave environments, the feedforward augmentation structure consistently delivers greater lifetime enhancement than its feedback counterpart. Among the nominal controllers considered, MPC-SP exhibits the strongest health-aware performance, offering substantial flexibility in adjusting the trade-off between energy and lifetime, while MPC-ZOH and LiTe-Con are comparatively less flexible. Simulation results highlight the generality of the proposed framework and its ability to adapt to different nominal WEC controllers. Nevertheless, the simulations also revealed important limitations for irregular waves. For MPC-ZOH, convexity issues arise even at moderate trade-off values (e.g., $q = -0.5$), while both LiTe-Con and MPC-SP fail to provide health-aware outcomes at extreme values (e.g., $q = -0.9$ or $q = -1$). The root cause lies in the fixed-delay mechanism: while the delay τ aligns destructively with the excitation force peak period in regular waves, it cannot consistently achieve

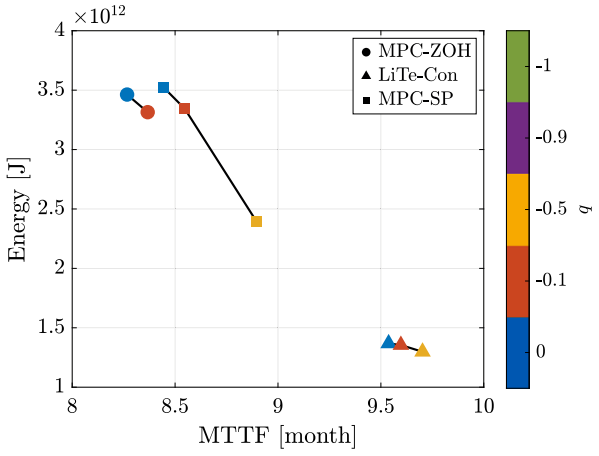

Fig. 10. Energy and MTTF values for a six-year period and different q in the irregular wave condition. Various controllers, such as the MPC-ZOH (circle), MPC-SP (square), and LiTE-Con (triangle), are utilised as nominal controllers within the feedforward control augmentation structure.

destructive interference in irregular waves, leading to cases where the augmented control input degrades reliability, rather than improving it. To overcome this limitation, future work will focus on developing an event-triggered control augmentation mechanism that selectively deactivates the augmentation whenever the augmented control input exceeds the nominal input in magnitude. Such a mechanism would extend the operational freedom of the proposed framework in irregular waves. In addition, further research will explore dynamic selection of q based on economic metrics, such as the price of electricity, enabling real-time decisions tailored to operational priorities, i.e. whether to favour extended lifetime or maximised energy capture.

CRediT authorship contribution statement

Amin Ziaei: Writing – original draft, Visualization, Software, Methodology, Investigation, Conceptualization. **Hafiz Ahsan Said:** Writing – review & editing, Supervision, Methodology, Conceptualization. **John V. Ringwood:** Writing – review & editing, Supervision, Funding acquisition, Conceptualization.

Declaration of competing interest

The authors declare that they have no known competing financial interests or personal relationships that could have appeared to influence the work reported in this paper.

Acknowledgements

This work was supported by Taighde Éireann (Research Ireland) under Grant No. 21/FFP-A/8997 and through the Marine Renewable Ireland (MaREI) Centre under Grant 12/RC/2302_P2.

Appendix. Proof of Lemma 1

Consider a nominal linear controller with the following general, stable, state-space representation:

$$\begin{cases} \dot{\boldsymbol{x}}_c(t) = \boldsymbol{A}_c \boldsymbol{x}_c(t) + \boldsymbol{B}_{c1} \begin{bmatrix} y_v(t) \\ y_z(t) \end{bmatrix} + \boldsymbol{B}_{c2} f_{ex}(t), \\ f_{PTO}^{nom}(t) = \boldsymbol{C}_c \boldsymbol{x}_c(t), \end{cases} \tag{A.1}$$

where $x_c(t)$ is the controller state vector. Throughout this appendix, we assume that the controller system matrix $\boldsymbol{A}_c$ is *Hurwitz*. Therefore, (13) is obtained as:

$$\begin{cases} \dot{\boldsymbol{x}}(t) = \boldsymbol{A}\boldsymbol{x}(t) + \boldsymbol{B}_1 f_{PTO}^{nom}(t) + \boldsymbol{B}_2 f_{ex}(t), \\ y_v(t) = \boldsymbol{C}_v \boldsymbol{x}(t), \quad y_z(t) = \boldsymbol{C}_z x(t). \end{cases} \tag{A.2}$$

Define the augmented state vector as $x_{aug}(t) = \begin{bmatrix} x(t) \\ x_c(t) \end{bmatrix}$, which evolves according to:

$$\dot{\boldsymbol{x}}_{aug}(t) = \boldsymbol{A}_{aug} \boldsymbol{x}_{aug}(t) + \boldsymbol{B}_{aug} f_{ex}(t), \tag{A.3}$$

where

$$\boldsymbol{A}_{aug} = \begin{bmatrix} \boldsymbol{A} & \boldsymbol{B}_1 \boldsymbol{C}_c \\ \boldsymbol{B}_{c1} \begin{bmatrix} \boldsymbol{C}_v \\ \boldsymbol{C}_z \end{bmatrix} & \boldsymbol{A}_c \end{bmatrix}, \quad \boldsymbol{B}_{aug} = \begin{bmatrix} \boldsymbol{B}_2 \\ \boldsymbol{B}_{c2} \end{bmatrix}.$$

Now, if the augmented linear system is shifted with the period of $f_{ex}(t)$ (assuming regular waves), i.e., T_0 in Assumption 1, $\dot{\boldsymbol{x}}_{aug}(t+T_0)$ yields:

$$\dot{\boldsymbol{x}}_{aug}(t+T_0) = \dot{\boldsymbol{x}}_{aug}(t). \tag{A.4}$$

On the other hand, $\boldsymbol{x}_{aug}$, the solution of (A.3), can be obtained [28] as:

$$\boldsymbol{x}_{aug}(t) = e^{\boldsymbol{A}_{aug}(t-t_0)} \boldsymbol{x}_{aug}(t_0) + \int_{t_0}^{t} e^{\boldsymbol{A}_{aug}(t-\zeta)} \boldsymbol{B}_{aug} \boldsymbol{f}_{ex}(\zeta) d\zeta, \tag{A.5}$$

where t_0 is the initial time. So, $\boldsymbol{x}_{aug}(t+T_0)$ is calculated as:

$$\begin{aligned} \boldsymbol{x}_{aug}(t+T_0) &= e^{\boldsymbol{A}_{aug}(t+T_0-t_0)} \boldsymbol{x}_{aug}(t_0) \\ &\quad + \int_{t_0}^{t+T_0} e^{\boldsymbol{A}_{aug}(t+T_0-\zeta)} \boldsymbol{B}_{aug} \boldsymbol{f}_{ex}(\zeta) d\zeta, \\ &= e^{\boldsymbol{A}_{aug}(t+T_0-t_0)} \boldsymbol{x}_{aug}(t_0) \\ &\quad + \int_{t_0}^{t} e^{\boldsymbol{A}_{aug}(t+T_0-\zeta)} \boldsymbol{B}_{aug} \boldsymbol{f}_{ex}(\zeta) d\zeta \\ &\quad + \int_{t}^{t+T_0} e^{\boldsymbol{A}_{aug}(t+T_0-\zeta)} \boldsymbol{B}_{aug} \boldsymbol{f}_{ex}(\zeta) d\zeta \\ &= e^{\boldsymbol{A}_{aug} T_0} x_{aug}(t) \\ &\quad + \int_{t}^{t+T_0} e^{\boldsymbol{A}_{aug}(t+T_0-\zeta)} \boldsymbol{B}_{aug} \boldsymbol{f}_{ex}(\zeta) d\zeta \end{aligned} \tag{A.6}$$

Now, $\boldsymbol{x}_{aug}(t) \equiv \boldsymbol{x}_{aug}(t+T_0)$ yields:

$$x_{aug}(t) = \left(\boldsymbol{I} - e^{\boldsymbol{A}_{aug} T_0} \right)^{-1} \int_{t}^{t+T_0} e^{\boldsymbol{A}_{aug}(t+T_0-\zeta)} \boldsymbol{B}_{aug} f_{ex}(\zeta) d\zeta. \tag{A.7}$$

Therefore, (A.7) results in the periodicity of $\boldsymbol{x}_{aug}(t) \Rightarrow \boldsymbol{x}_c(t) \Rightarrow f_{PTO}^{nom}(t)$, if $\boldsymbol{A}_{aug}$ is *Hurwitz*.

For the feedforward energy-maximising WEC controllers, such as LiTe-Con and MPC-SP, $\boldsymbol{A}_{aug}$ is always *Hurwitz*, since A_{aug} yields an upper triangular matrix as:

$$\boldsymbol{A}_{aug} = \begin{bmatrix} \boldsymbol{A} & \boldsymbol{B}_1 \boldsymbol{C}_c \\ \boldsymbol{0} & \boldsymbol{A}_c \end{bmatrix}. \tag{A.8}$$

However, for a feedback energy-maximising WEC controller, such as MPC-ZOH, $\boldsymbol{B}_{c1}$ determines whether $\boldsymbol{A}_{aug}$ is *Hurwitz*. For example, for the MPC-ZOH in (24), the undisturbed closed-loop system can be asymptotically stable (i.e., $\boldsymbol{A}_{aug}$ remains Hurwitz) through appropriate tuning of the control penalty parameter r. Specifically, choosing a sufficiently large r leads to moderate control action, preserving closed-loop asymptotic stability. The proof is complete.

Data availability

No data was used for the research described in the article.

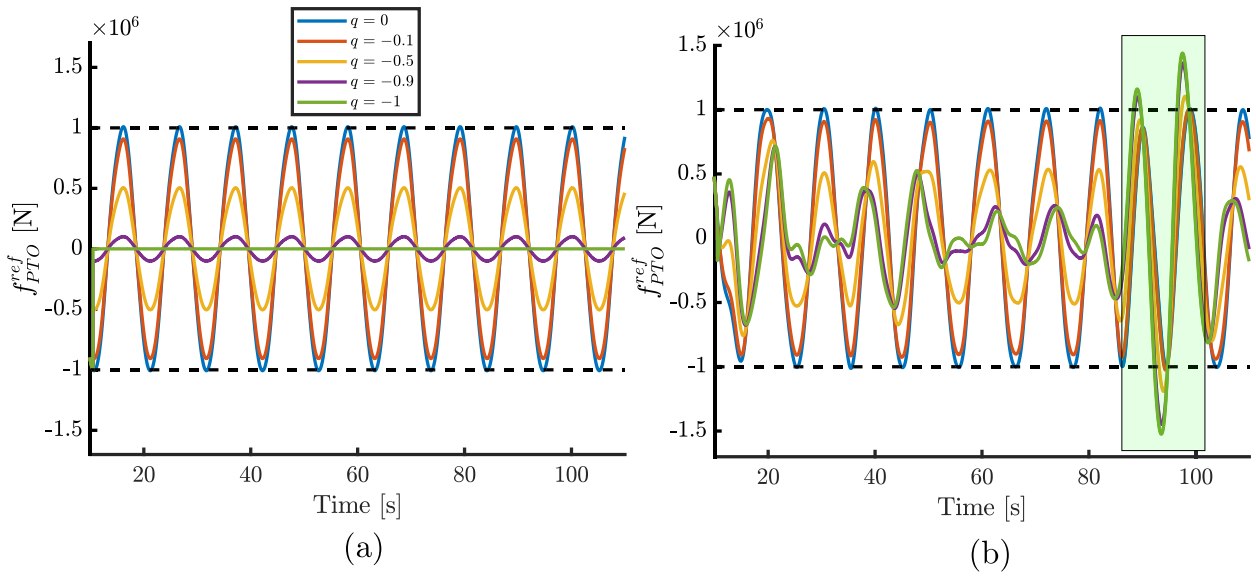

Fig. 11. Comparison of Control input graphs for different q in the feedforward control augmentation structure with MPC-SP as a nominal controller in the (a) regular and (b) irregular waves.

References

[1] Li X. Diversification and localization of energy systems for sustainable development and energy security. Energy Policy 2005;33(17):2237–43.
[2] Reguero B, Losada I, Méndez F. A global wave power resource and its seasonal, interannual and long-term variability. Appl Energy 2015;148:366–80.
[3] International Energy Agency (IEA). Electricity — Global energy review 2025. 2025, [Accessed 6 October 2025], https://www.iea.org/reports/global-energy-review-2025/electricity.
[4] Said HA, Costello S, Ringwood J. On the complementarity of wave, tidal, wind and solar resources in Ireland. In: Proceedings of the European wave and tidal energy conference. vol. 15, Bilbao, Spain; 2023, p. 1–6.
[5] Said HA, Skiarski A, Ringwood JV. Combined renewable resource exploitation: Implications for the all-island irish electricity supply system. Energy Convers Manag: X 2025;26:100992.
[6] Astariz S, Iglesias G. The economics of wave energy: A review. Renew Sustain Energy Rev 2015;45:397–408.
[7] Sørensen JD. Framework for risk-based planning of operation and maintenance for offshore wind turbines. Wind Energy 2009;12(5):493–506.
[8] Ambühl S, Marquis L, Kofoed JP, Sørensen JD. Operation and maintenance strategies for wave energy converters. Proc Inst Mech Eng Part O: J Risk Reliab 2015;229(5):417–41.
[9] Ringwood JV, Zhan S, Faedo N. Empowering wave energy with control technology: Possibilities and pitfalls. Annu Rev Control 2023;55:18–44.
[10] Kadry S. Diagnostics and prognostics of engineering systems: Methods and techniques. IGI Global; 2012.
[11] Said HA, Sardá AC, Ringwood JV. Fault management in wave energy systems: Diagnosis, prognosis, and fault-tolerant control. Ocean Eng 2025;316:119794.
[12] Papini G, Faedo N, Mattiazzo G. Fault diagnosis and fault-tolerant control in wave energy: A perspective. Renew Sustain Energy Rev 2024;199:114507.
[13] Do MH, Söffker D. State-of-the-art in integrated prognostics and health management control for utility-scale wind turbines. Renew Sustain Energy Rev 2021;145:111102.
[14] Yang B, Duan J, Chen Y, Wu S, Li M, Cao P, Jiang L. A critical survey of power take-off systems based wave energy converters: Summaries, advances, and perspectives. Ocean Eng 2024;298:117149.
[15] Papini G, Faedo N, Mattiazzo G. Accommodating sensor faults in wave energy optimal control. IFAC Pap 2024;58(4):586–91.
[16] Yang S-H, Ringsberg JW, Johnson E, Hu Z. Biofouling on mooring lines and power cables used in wave energy converter systems—Analysis of fatigue life and energy performance. Appl Ocean Res 2017;65:166–77.
[17] Davidson J, Genest R, Ringwood JV. Adaptive control of a wave energy converter. IEEE Trans Sustain Energy 2018;9(4):1588–95.
[18] Ziaei A, Said HA, Ringwood JV. Health-sensitive control of wave energy converters: A primer. Ocean Eng 2024;311:118893.
[19] Ziaei A, Said HA, Ringwood JV. Health aware control of wave energy converters: Possibilities and challenges. In: Proceedings of the 6th international conference on renewable energies offshore. Lisbon, Portugal; 2024, p. 1–9.
[20] Ziaei A, Said HA, Ringwood JV. Health-aware control augmentation for wave energy converters using a reliability metric. In: European wave and tidal energy conference. Madeira, Portugal; 2025, p. 1–9.
[21] Peng B, Gu N, Wang D, Li T, Han B, Peng Z. Online learning-based active disturbance rejection control of autonomous surface vehicles with HIL simulations. Ocean Eng 2023;288:116041.
[22] Srinidhi A, Raja R, Alzabut J, Bagdasar O. Memory-based sampled-data control scheme for vehicle seat suspension system with actuator faults via a looped Lyapunov approach. Internat J Robust Nonlinear Control 2025.
[23] Zhang C, Xiao B, Wu J, Li B. On low-complexity control design to spacecraft attitude stabilization: An online-learning approach. Aerosp Sci Technol 2021;110:106441.
[24] Ziaei A, Sinafar B, Kharrati H, Rahimi A. Concurrent-learning-based event-triggered fault tolerant attitude control for spacecraft with actuator faults. Adv Space Res 2024;73(1):95–107.
[25] Zhang C, Lu W, Zhao S, Wu J, Zhu X, Liu Z, He W. Enhancing attitude tracking with self-learning control using tanh-type learning intensity. IEEE Trans Autom Sci Eng 2025;22:16976–86.
[26] García-Violini D, Faedo N, Jaramillo-Lopez F, Ringwood JV. Simple controllers for wave energy devices compared. J Mar Sci Eng 2020;8(10):793.
[27] Faedo N, Olaya S, Ringwood JV. Optimal control, MPC and MPC-like algorithms for wave energy systems: An overview. IFAC J Syst Control 2017;1:37–56.
[28] Ogata K, et al. Modern control engineering. Prentice Hall India; 2009.
[29] Giorgi G, Ringwood JV. Computationally efficient nonlinear Froude–Krylov force calculations for heaving axisymmetric wave energy point absorbers. J Ocean Eng Mar Energy 2017;3:21–33.
[30] Falnes J, Kurniawan A. Ocean waves and oscillating systems: Linear interactions including wave-energy extraction, vol. 8, Cambridge University Press; 2020.
[31] Brebbia CA. The boundary element method in enginering practice. Eng Anal 1984;1:3–12.
[32] Babarit A, Delhommeau G. Theoretical and numerical aspects of the open source BEM solver NEMOH. In: European wave and tidal energy conference. Nantes, France; 2015.
[33] Lee C-H. WAMIT theory manual. Massachusetts Institute of Technology, Department of Ocean Engineering; 1995.
[34] Mérigaud A, Ringwood JV. Free-surface time-series generation for wave energy applications. IEEE J Ocean Eng 2017;43(1):19–35.
[35] Peña-Sanchez Y, Faedo N, Penalba M, Giorgi G, Mérigaud A, Windt C, Violini DG, Wang L, Ringwood JV. Finite-order hydrodynamic approximation by moment-matching (FOAMM) toolbox for wave energy applications. In: Proceedings of the 13th European wave and tidal energy conference. EWTEC, Naples, Italy; 2019, p. 1448–:1448–9.
[36] Rausand M, Hoyland A. System reliability theory: Models, statistical methods, and applications, vol. 396, John Wiley & Sons; 2003.
[37] Goble WM. Control systems safety evaluation and reliability. ISA; 2010.
[38] Cox DR. Regression models and life-tables. J R Stat Soc Ser B Stat Methodol 1972;34(2):187–202.
[39] Chamseddine A, Theilliol D, Sadeghzadeh I, Zhang Y, Weber P. Optimal reliability design for over-actuated systems based on the MIT rule: Application to an octocopter helicopter testbed. Reliab Eng Syst Saf 2014;132:196–206.
[40] Salazar JC, Sanjuan A, Nejjari F, Sarrate R. Health-aware control of an octorotor UAV system based on actuator reliability. In: 4th international conference on control, decision and information technologies. coDIT, Barcelona, Spain: IEEE; 2017, p. 0815–20.

[41] Salazar JC, Sarrate R, Nejjari F, Weber P, Theilliol D. Reliability computation within an MPC health-aware framework. IFAC Pap 2017;50(1):12230–5.
[42] Zhang J, Liu T, Qiao J. Solving a reliability-performance balancing problem for control systems with degrading actuators under model predictive control framework. J Franklin Inst 2022;359(9):4260–87.
[43] Garcia CE, Prett DM, Morari M. Model predictive control: Theory and practice—A survey. Automatica 1989;25(3):335–48.
[44] Åström KJ, Wittenmark B. Computer controlled systems: Theory and design. Prentice-Hall: Englewood Cliffs, NJ; 1990.
[45] Li G, Belmont MR. Model predictive control of sea wave energy converters–Part I: A convex approach for the case of a single device. Renew Energy 2014;69:453–63.
[46] Papini G, Paduano B, Pasta E, Carapellese F, Mattiazzo G, Faedo N. On the influence of mooring systems in optimal predictive control for wave energy converters. Renew Energy 2023;218:119242.
[47] Kwon WH, Han SH. Receding horizon control: Model predictive control for state models. Springer Science & Business Media; 2005.
[48] Bacelli G, Ringwood JV. Numerical optimal control of wave energy converters. IEEE Trans Sustain Energy 2014;6(2):294–302.
[49] Genest R, Ringwood JV. Receding horizon pseudospectral control for energy maximization with application to wave energy devices. IEEE Trans Control Syst Technol 2016;25(1):29–38.
[50] Peña-Sanchez Y, Windt C, Davidson J, Ringwood JV. A critical comparison of excitation force estimators for wave-energy devices. IEEE Trans Control Syst Technol 2019;28(6):2263–75.
[51] García-Violini D, Ringwood JV. Robust control of wave energy converters using spectral and pseudospectral methods: a case study. In: 2019 American control conference. ACC, Philadelphia, PA, USA: IEEE; 2019, p. 4779–84.
[52] García-Violini D, Peña-Sanchez Y, Faedo N, Ringwood JV. An energy-maximising linear time invariant controller (LiTe-Con) for wave energy devices. IEEE Trans Sustain Energy 2020;11(4):2713–21.
[53] Faedo N, Peña-Sanchez Y, Ringwood JV. Finite-order hydrodynamic model determination for wave energy applications using moment-matching. Ocean Eng 2018;163:251–63.
[54] García-Violini D, Peña-Sanchez Y, Faedo N, Ferri F, Ringwood JV. A broadband time-varying energy maximising control for wave energy systems (LiTe-Con+): Framework and experimental assessment. IEEE Trans Sustain Energy 2023;14(3):1516–25.
[55] Na J, Wang B, Li G, Zhan S, He W. Nonlinear constrained optimal control of wave energy converters with adaptive dynamic programming. IEEE Trans Ind Electron 2018;66(10):7904–15.
[56] Mosquera F, Faedo N, Evangelista C, Puleston P, Ringwood J. Energy-maximising tracking control for a nonlinear heaving point absorber system commanded by second order sliding modes. IFAC Pap 2022;55(31):357–62.
[57] Hasselmann K, Barnett TP, Bouws E, Carlson H, Cartwright DE, Enke K, Ewing J, Gienapp A, Hasselmann D, Kruseman P, et al. Measurements of wind-wave growth and swell decay during the Joint North Sea Wave Project (JONSWAP). Ergänzungsheft Deutschen Hydrogr Zeitschrift 1973;8(12):1–95.
[58] Marine Institute. AMETS–weather buoy. 2025, Accessed 18 August 2025, https://www.marine.ie/site-area/data-services/real-time-observations/amets-weather-buoy.
[59] Faedo N, Dores Piuma FJ, Giorgi G, Ringwood JV. Nonlinear model reduction for wave energy systems: a moment-matching-based approach. Nonlinear Dynam 2020;102(3):1215–37.
[60] Peña-Sanchez Y, Mérigaud A, Ringwood JV. Short-term sea elevation forecasting for wave energy applications: The AR model revisited. IEEE J Ocean Eng 2020;45(2):462–71.
[61] Mueller M, Lopez R, McDonald A, Jimmy G. Reliability analysis of wave energy converters. In: International conference on renewable energy research and applications. ICRERA, Birmingham, United Kingdom: IEEE; 2016, p. 667–72.